catalysts

MDPI

Article

Theoretically Predicted CO Adsorption and Activation on the Co-Doped hcp-Fe_7C_3 Catalyst

Yajing Duan [1], Huijuan Sun [1], Hui Du [2] and Wencai Lu [1,*]

[1] College of Physics, Qingdao University, Qingdao 266071, China
[2] College of Chemistry and Chemical Engineering, Institute for Sustainable Energy and Resources, Qingdao University, Qingdao 266071, China
* Correspondence: wencailu@jlu.edu.cn

Abstract: The Hcp-Fe_7C_3 phase has attracted more attention due to the high catalytic activity in Fischer–Tropsch synthesis (FTS) reactions. In this work, the adsorption and activation of CO on a Co-doped hcp-Fe_7C_3 catalyst were investigated by density functional theory (DFT) in order to understand the effect of Co doping on the initial step of FTS reactions on iron-based catalysts. Different Co-doped hcp-Fe_7C_3 (001) and $(1\bar{1}0)$ surfaces were constructed, and the CO adsorption configurations were studied. The calculated results show that the structure of the (001) surface remains basically unchanged after doping with Co atoms, while the replacement of Fe or C atoms on $(1\bar{1}0)$ surfaces with Co atoms has a significant impact on the surface structure. The top sites on the doped Co atoms of hcp-Fe_7C_3 are disadvantages for the CO adsorption, whereas the T, 2F, or 3F sites around the doped Co atoms are beneficial for promoting the adsorption of CO. The CO direct dissociation pathways on the four types of Co-doped hcp-Fe_7C_3 (001) surfaces are exothermic, while the H-assisted dissociation pathways of CO are endothermic. The H-assisted activation via HCO on the 3F1 site of the 2Co2-doped hcp-Fe_7C_3 (001) surface shows the lowest energy barrier of 1.96 eV. For the Co-doped hcp-Fe_7C_3 $(1\bar{1}0)$ surfaces, the H-assisted activation via HCO is the preferred activation pathway for CO on the Co-doped surfaces with the energy barrier of approximately 1.30 eV.

Keywords: hcp-Fe_7C_3; Fischer–Tropsch synthesis; CO adsorption and activation; density functional theory; Co-doped

Citation: Duan, Y.; Sun, H.; Du, H.; Lu, W. Theoretically Predicted CO Adsorption and Activation on the Co-Doped hcp-Fe_7C_3 Catalyst. *Catalysts* **2023**, *13*, 564. https://doi.org/10.3390/catal13030564

Academic Editors: Guangchao Liang and Charles Edwin Webster

Received: 12 February 2023
Revised: 8 March 2023
Accepted: 9 March 2023
Published: 11 March 2023

1. Introduction

Fischer–Tropsch synthesis (FTS) is a promising process for the conversion of syngas (from coal, biomass, and natural gas) into clean liquid fuels and chemicals [1–5]. Syngas, CO, and H_2 convert to mainly alkanes and olefins through a series of catalytic reactions as well as converting to oxygenated chemicals, such as alcohols, aldehydes, ketones, acids, etc. [6]. Two major categories, iron-based and cobalt-based catalysts, were widely used in industrial FTS processes [7–9]. The iron-based catalysts have been widely used in FTS processes on account of the superiorities of high activity, low cost, operational flexibility, and raw material adaptability [7,10,11]. Contrary to the lower catalytic activity toward long-chain hydrocarbons of iron-based catalysts, the much more expensive cobalt-based catalysts show high activity and selectivity [12–14].

Recently, iron carbides, such as χ-Fe_5C_2, Fe_7C_3, θ-Fe_3C, and ε-Fe_2C, were suggested as the active phases of iron-based catalysts during the FTS processes [15–21]. However, the density functional theory (DFT) study of carbides catalysts has demonstrated that the theoretically intrinsic selectivity toward long-chain hydrocarbons of iron carbides was higher than that of cobalt at relatively low reaction temperatures [22,23]. In practice, the observed lower selectivity toward long-chain hydrocarbons of iron carbides was caused by the high reaction temperature required for CO dissociation. Therefore, many efforts have been attempted to fabricate Co-doped iron-based catalysts in order to realize a high

activity and selectivity at a relatively low temperature. Yang et al., fabricated the Fe_5C_2/Co heterostructured nanoparticles for low temperature FTS and studied the synergistic effects between Fe_5C_2 and Co parts in the catalysts [24]. In the Fe_5C_2/Co heterostructured nanocatalysts, Co was responsible for the CO dissociation, while Fe_5C_2 was responsible for the chain growth, which led to the enhanced catalytic performance in low temperature FTS reactions.

The FTS reaction is an extremely complicated system because of the hundreds of elementary reactions which are all interconnected with each other on the surface of catalyst. Moreover, both activity and selectivity of the catalyst are very important in the catalytic system. There have been many studies published in the literature aimed at investigating the adsorption and activation mechanism of CO on iron carbides. It is generally known that the CO direct dissociation pathway is the major CO-activated mechanism on (510) surfaces of χ-Fe_5C_2 catalysts, while the CO H-assisted dissociation pathway is preferred on the (100) and (001) surfaces of χ-Fe_5C_2 [18,25,26]. For Fe_3C catalysts, the reported results revealed that CO direct dissociation is favored on the (110), (101), $(1\bar{1}1)$, and (111) surfaces, and the CO H-assisted dissociation pathway is favored on the (100), (011), $(0\bar{1}1)$, and (001) surfaces, while both of the two dissociation pathways are possible on (010) surfaces for the similar overall barriers [27].

Recently, the hcp-Fe_7C_3 phase has attracted more attention due to the high catalytic activity in FTS reactions. Chang et al., prepared different iron carbide phases by the pretreatment of a binary Fe/SiO_2 model catalysts at different gas atmospheres and found that Fe_7C_3 has the highest intrinsic activity among the three candidate carbides (ε-Fe_2C, Fe_7C_3, and χ-Fe_5C_2) in typical medium-temperature FTS conditions [20]. Zhang et al., studied the CO activation mechanism on hcp-Fe_7C_3 (211) and found that the top site and four-fold site are the major adsorption sites for CO, and the surface carbon is able to be the CO activation site by the CO insertion dissociation pathway. The CO was activated through the H-assisted dissociation pathway on the top site, while it was activated through the direct dissociation pathway on 4-fold site [28].

To the best of our knowledge, theoretical studies of the adsorption and activation mechanism of CO on Co-doped iron carbides have rarely been reported. Herein, the adsorption and dissociation mechanism of CO on the Co-doped hcp-Fe_7C_3 catalyst were investigated by DFT. Firstly, the different Co-doped hcp-Fe_7C_3 (001) and $(1\bar{1}0)$ surfaces were constructed. Then, the adsorption configurations of CO on different Co-doped hcp-Fe_7C_3 surfaces were calculated. Moreover, the dissociation pathway of CO on the most stable adsorption configurations of each Co-doped hcp-Fe_7C_3 surface are discussed.

2. Results and Discussion

2.1. Structures of Co-Doped hcp-Fe_7C_3 Surfaces

The selected (001) and $(1\bar{1}0)$ surfaces of hcp-Fe_7C_3 are demonstrated in Figure 1, which are modeled by a (2 × 2) supercell of periodical repeated slabs with a thickness of three repeated units and a vacuum layer of 15 Å. The upper layers are allowed to relax, while the bottom layers are kept at their bulk positions. As shown in Figure 1, the top layer of (001) surface consists only of Fe atoms, while the top layer of $(1\bar{1}0)$ surface consists of Fe and C atoms. As a result, the surface Fe and C atoms might be replaced by Co atoms to form the Co-doped hcp-Fe_7C_3 catalysts. Therefore, based on the considered symmetry of the hcp-Fe_7C_3 (001) surface, different surface Fe atoms are replaced by Co atoms to form four types of Co-doped hcp-Fe_7C_3 (001) surface, which are denoted as 1Co-doped (001), 2Co1-doped (001), 2Co2-doped (001), and 3Co-doped (001). On the (001) surface, the center site of hexagon (labeled as T4) locates in the hollow in the surface. Therefore, the Co-doped (001) surface with the Co at the T4 site is not discussed in our present work. For the more complicated composition of the hcp-Fe_7C_3 $(1\bar{1}0)$ surface, either Fe or C could be replaced by Co atoms, thus four types of Co-doped hcp-Fe_7C_3 $(1\bar{1}0)$ surface denoted as 1Co1-doped $(1\bar{1}0)$, 1Co2-doped $(1\bar{1}0)$, 1Co3-doped $(1\bar{1}0)$, and 2Co-doped $(1\bar{1}0)$ are obtained. The structures of different Co-doped hcp-Fe_7C_3 (001) and $(1\bar{1}0)$ surfaces are

shown in Figures 2 and 3, with *x*Co*y*-doped hcp-Fe_7C_3, where, in the names of Co-doped hcp-Fe_7C_3, *x* means the number of Co atoms, and *y* means the different types of Co-doped structures with the same number of Co atoms. It can be seen that the surface structure of (001) surface remains basically unchanged after doping with Co atoms. On the contrary, the replacement of Fe or C atoms on $(1\bar{1}0)$ surfaces with Co atoms has a significant impact on the surface structure.

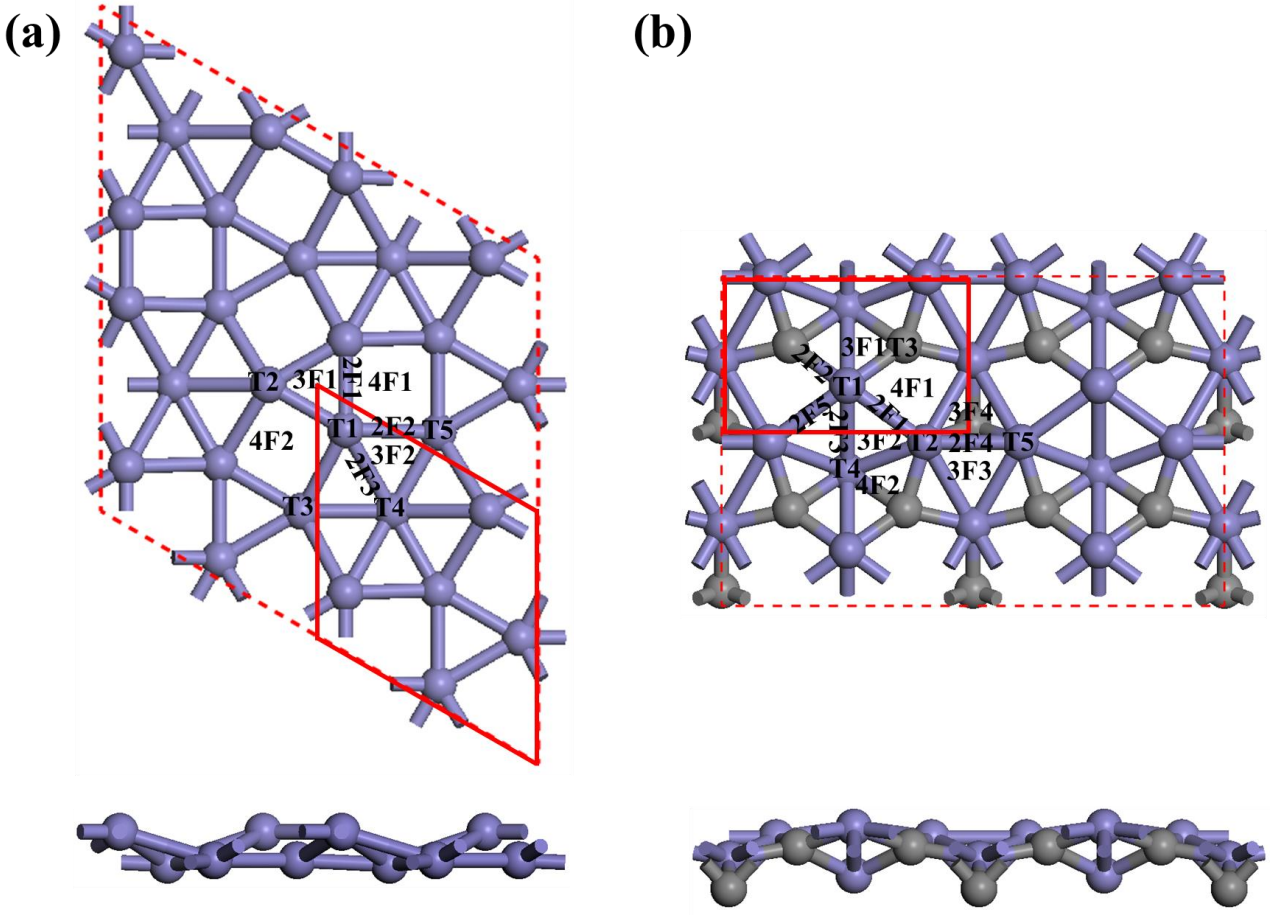

Figure 1. Top and side views of hcp-Fe_7C_3 (**a**) (001) and (**b**) $(1\bar{1}0)$ surfaces. The Fe and C atoms are colored purple and gray, respectively.

2.2. CO Adsorption on the Co-Doped hcp-Fe_7C_3 Surfaces

CO adsorption on FTS catalysts is critical for deep understanding of the catalytic reaction mechanism since the CO adsorption is the first step of the FTS reaction, which shows great influences on the C=O bond breaking and the subsequent chain reactions. The possible adsorption sites of CO on the hcp-Fe_7C_3 (001) and $(1\bar{1}0)$ surfaces are labeled in Figure 1, in which the top and n-fold sites are labeled as T, 2F, 3F, and 4F, respectively. For the original clean hcp-Fe_7C_3 (001) surface, the most stable adsorption site for CO is the 3F1 site with the adsorption energy of -2.47 eV [29]. The C-O bond length and the adsorption energies for CO on different Co-doped hcp-Fe_7C_3 (001) surfaces are listed in Table 1, and the most stable adsorption configurations of CO on different Co-doped hcp-Fe_7C_3 (001) surfaces are demonstrated in Figure 4.

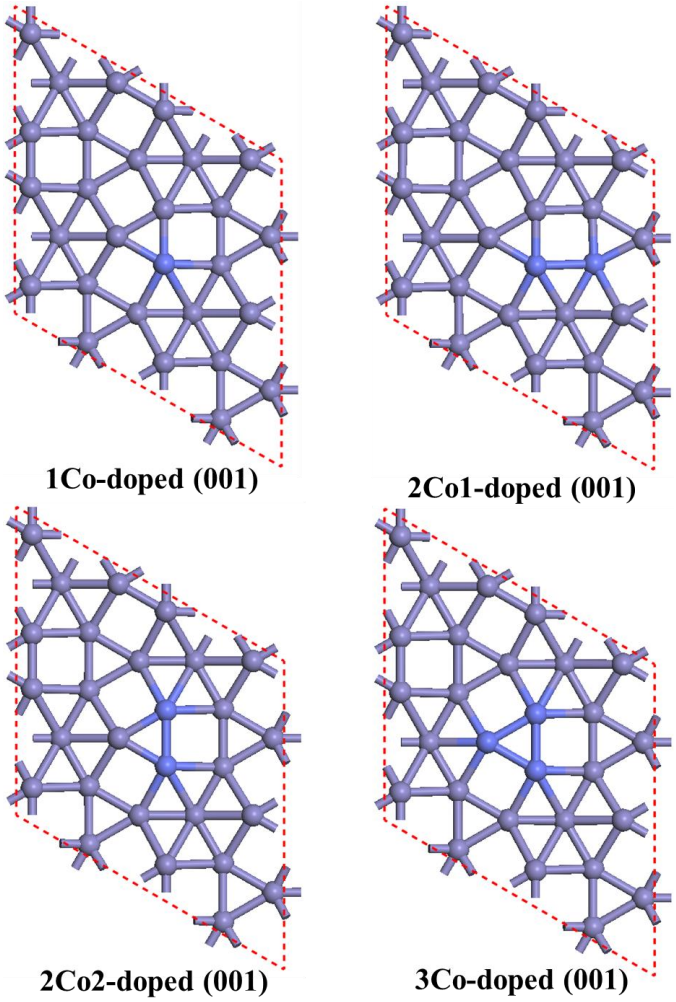

Figure 2. The structures of different Co-doped hcp-Fe_7C_3 (001) surfaces. The Fe, C, and Co atoms are colored purple, gray, and blue, respectively.

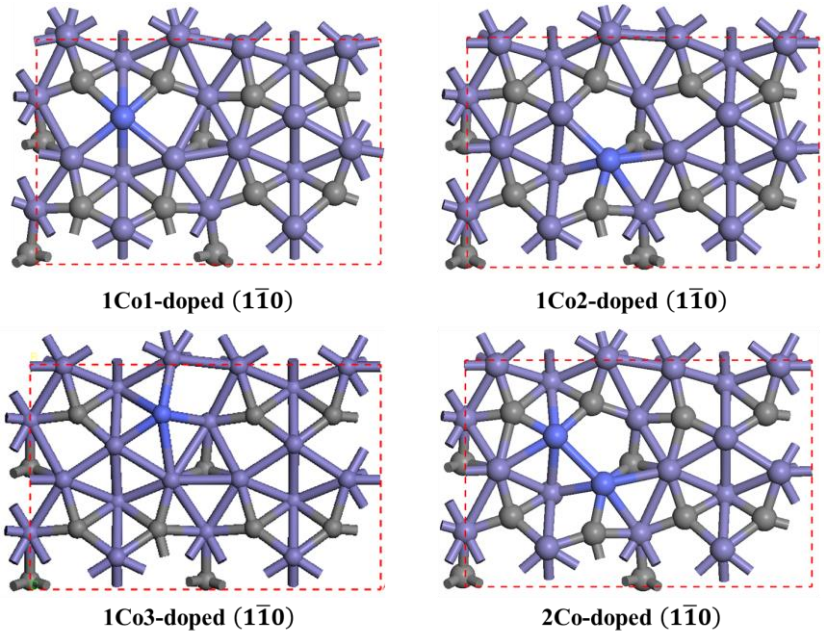

Figure 3. The structures of different Co-doped hcp-Fe_7C_3 (1$\bar{1}$0) surfaces. The Fe, C, and Co atoms are colored purple, gray, and blue, respectively.

Table 1. The C-O bond length and the adsorption energies for CO on the Co-doped hcp-Fe_7C_3 (001) surface.

Site	(001)		1Co-Doped (001)		2Co1-Doped (001)		2Co2-Doped (001)		3Co-Doped (001)	
	$d_{(C-O)}$/Å	E_{ads}/eV	$d_{(C-O)}$/Å	E_{ads}/eV	$d_{(C-O)}$/Å	E_{ads}/eV	$d_{(C-O)}$/Å	E_{ads}/eV	$d_{(C-O)}$/Å	E_{ads}/eV
T1			1.174	−2.23	1.175	−2.22	1.174	−2.20	1.176	−2.17
T2			1.176	−2.15	1.176	−2.14	1.178	−1.62	-	-
T3			1.177	−2.12	1.177	−2.14	1.177	−1.98	1.186	−1.94
T4			1.181	−2.40	1.181	−2.03	1.175	−1.75	1.190	−2.33
T5			- *	-	1.180	−1.84	1.201	−2.38	-	-
2F1			1.201	−2.47	1.185	−2.01	1.201	−2.58	1.199	−2.27
2F2			1.179	−2.12	1.190	−1.83	1.202	−2.60	1.195	−2.30
2F3			1.181	−2.14	1.196	−2.54	1.186	−2.29	1.201	−2.38
3F1	1.202	−2.47	1.203	−2.48	1.203	−2.50	1.201	−2.61	1.200	−2.26
3F2			1.181	−2.40	1.201	−2.53	1.198	−2.34	1.204	−2.37
4F1			1.198	−2.04	1.203	−2.02	1.231	−2.08	1.233	−2.08
4F2			1.193	−2.11	1.191	−2.16	1.295	−2.17	-	-

*—denotes the equivalent symmetrical sites.

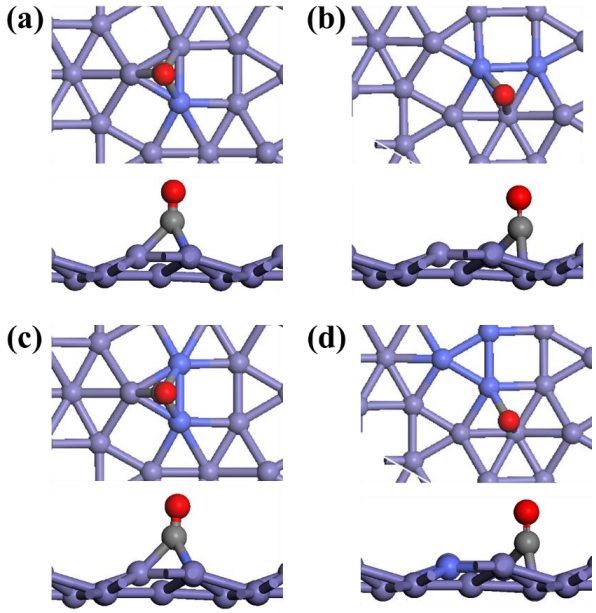

Figure 4. Top and side views of the most stable adsorption configurations of CO on (**a**) 1Co-doped (001), (**b**) 2Co1-doped (001), (**c**) 2Co2-doped (001), and (**d**) 3Co-doped (001) surfaces. The Fe, Co, C, and O atoms are colored purple, blue, gray, and red, respectively.

For the 1Co-doped (001) surface, the most stable adsorption site for CO is the 3F1 site with the lowest adsorption energy of −2.48 eV, which is approximately the same as the clean hcp-Fe_7C_3 (001) surface. The 3F1 site provides three bond connections to the adsorbed CO molecule, resulting in the longest C-O bond length of 1.203 Å. In contrast, the adsorption energy of CO on the top site of Co atom (T1 site) is −2.23 eV, and the C-O bond length is 1.174 Å, indicating the inferior adsorbability of surface Co atoms for CO. The results show that the replacement of the hcp-Fe_7C_3 (001) surface with a single Co atom rarely changes the interactions between the (001) surface and CO.

With the increasing Co content of the (001) surface, there are great changes taking place in the adsorption behavior of CO on Co-doped (001) surfaces. For the hcp-Fe_7C_3 (001) surface replaced with two Co atoms, their adsorbabilities for CO are enhanced to various degrees. The most stable adsorption site for CO on 2Co1-doped (001) is changed to the 2F3 site with the adsorption energy of −2.54 eV and the C-O bond length of 1.196 Å, but it is still energetically favorable for CO adsorption compared to the clean hcp-Fe_7C_3

(001) surface. Although the 3F1 site is less stable than the 2F3 site, the corresponding adsorption energy −2.50 eV is still lower than that of the clean hcp-Fe_7C_3 (001) surface. For the 2Co2-doped (001) surface, the most stable adsorption site is the 3F1 site with the adsorption energy of −2.61 eV and the C-O bond length of 1.201 Å, which shows the strongest interaction between the four types of Co-doped hcp-Fe_7C_3 (001) surfaces and CO. On the basis of the structure of the 1Co-doped (001) surface, the 3Co-doped (001) structure containing three symmetrical Co atoms was constructed. The most stable adsorption site for CO is the 2F3 site with the lowest adsorption energy of −2.38 eV, and the corresponding C-O bond length is 1.201 Å.

As a result, the top sites on the doped Co atoms of hcp-Fe_7C_3 (001) are disadvantages for the CO adsorption, whereas the 2F site or 3F site around the doped Co atoms are beneficial for promoting the adsorption of CO.

The replacement of Fe or C atoms on $(1\bar{1}0)$ surface with Co atoms has a significant impact on the surface structure. For the original clean hcp-Fe_7C_3 $(1\bar{1}0)$ surface, the most stable adsorption site for CO is the T1 site with the adsorption energy of −2.49 eV. The C-O bond length and the adsorption energies for CO on different Co-doped hcp-Fe_7C_3 $(1\bar{1}0)$ surfaces are listed in Table 2, and the most stable adsorption configurations of CO on different Co-doped hcp-Fe_7C_3 $(1\bar{1}0)$ surfaces are demonstrated in Figure 5.

Table 2. The C-O bond length and the adsorption energies for CO on the Co-doped hcp-Fe_7C_3 $(1\bar{1}0)$ surface.

Site	$(\bar{1}10)$		1Co1-Doped $(\bar{1}10)$		1Co2-Doped $(\bar{1}10)$		1Co3-Doped $(\bar{1}10)$		2Co-Doped $(\bar{1}10)$	
	$d_{(C-O)}$/Å	E_{ads}/eV	$d_{(C-O)}$/Å	E_{ads}/eV	$d_{(C-O)}$/Å	E_{ads}/eV	$d_{(C-O)}$/Å	E_{ads}/eV	$d_{(C-O)}$/Å	E_{ads}/eV
T1	1.180	−2.49	1.178	−1.97	1.187	−3.26	1.181	−2.33	1.175	−2.01
T2			1.177	−1.95	1.179	−1.84	1.172	−1.91	1.175	−1.82
T3			1.178	−1.88	1.173	−1.81	1.176	−2.15	1.170	−1.62
T4			1.171	−1.90	1.177	−1.92	1.179	−1.88	1.186	−2.04
T5			-*	-	1.182	−2.18	-	-	1.181	−2.00
2F1			1.196	−2.02	1.194	−1.89	1.181	−1.88	1.194	−2.01
2F2			1.175	−1.81	-	-	1.177	−1.83	-	-
2F3			1.181	−1.89	1.187	−1.91	1.187	−1.91	1.190	−1.98
2F4			-	-	1.181	−2.11	1.173	−2.02	1.192	−1.91
2F5			-	-	1.176	−1.82	1.184	−1.93	1.196	−2.21
3F1			1.182	−1.89	-	-	1.196	−1.86	1.175	−1.87
3F2			1.184	−1.94	1.180	−1.87	1.179	−1.95	1.153	−2.01
3F3			-	-	1.179	−1.85	1.182	−1.88	1.177	−1.79
3F4			-	-	-	-	1.190	−1.93	-	-
4F1			1.188	−1.87	1.185	−1.99	1.186	−1.98	1.194	−1.87
4F2			-	-	1.190	−2.04	-	-	1.255	−1.74

*—denotes the sites that were not calculated.

For the 1Co1-doped $(1\bar{1}0)$ surface, the most stable adsorption site for CO is the 2F1 site with the lowest adsorption energy of −2.02 eV and the longest C-O bond length of 1.196 Å, which is higher than that of the clean hcp-Fe_7C_3 $(1\bar{1}0)$ surface. However, for the 1Co2-doped $(1\bar{1}0)$ surface, the most stable adsorption site for CO is the T1 site with the lowest adsorption energy of −3.26 eV, which is much lower than that of the clean hcp-Fe_7C_3 $(1\bar{1}0)$ surface, indicating the strong adsorbability of surface Fe atoms for CO. When the C atom on $(1\bar{1}0)$ surface is replaced with the Co atom, the surface structure of hcp-Fe_7C_3 $(1\bar{1}0)$ surface is slightly changed. The most stable adsorption site for CO is still the T1 site with the lowest adsorption energy of −2.33 eV on the 1Co3-doped $(1\bar{1}0)$ surface.

With the increasing Co content of $(1\bar{1}0)$ surface, the most stable adsorption site for CO on 2Co-doped $(1\bar{1}0)$ is changed to the 2F5 site with the adsorption energy of −2.21 eV and the C-O bond length of 1.196 Å, which is energetically unfavorable for CO adsorption compared to the clean hcp-Fe_7C_3 $(1\bar{1}0)$ surface. Similar to the Co-doped (001) surfaces, the top sites on the doped Co atoms of hcp-Fe_7C_3 $(1\bar{1}0)$ are disadvantages for the CO

adsorption, but the T1 site on the 1Co2-doped $(1\bar{1}0)$ surface shows the strongest interaction between the four types of Co-doped hcp-Fe_7C_3 $(1\bar{1}0)$ surfaces and CO.

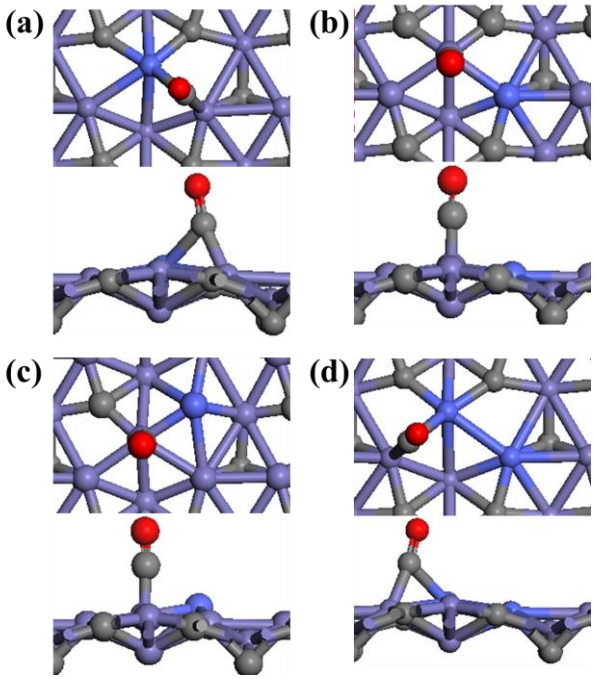

Figure 5. Top and side views of the most stable adsorption configurations of CO on (**a**) 1Co1-doped $(1\bar{1}0)$, (**b**) 1Co2-doped $(1\bar{1}0)$, (**c**) 1Co3-doped $(1\bar{1}0)$, and (**d**) 2Co-doped $(1\bar{1}0)$ surfaces. The Fe, Co, C, and O atoms are colored purple, blue, gray, and red, respectively.

2.3. CO Activation on the Co-Doped hcp-Fe_7C_3 Surfaces

CO activation has been proved to be the critical step of the FTS reaction pathway. After the chemical adsorption of CO on the catalyst surface, the CO activation pathways mainly include two categories, the CO direct dissociation and H-assisted dissociation. With the former, CO dissociates into reactive C and O species. For the latter, with the effect of reactive H species, CO dissociates into HCO or COH species. In the present work, the CO direct dissociation and H-assisted dissociation pathways on the most stable sites of Co-doped hcp-Fe_7C_3 (001) and $(1\bar{1}0)$ surfaces are compared. The potential energy diagrams, including the elemental reaction barrier (E_a) and reaction energy (ΔE_r), for the activation of CO on the Co-doped hcp-Fe_7C_3 surfaces are demonstrated in Figure 6. The structures of the transition states for CO direct dissociation and H-assisted dissociation pathways on the most stable site of Co-doped hcp-Fe_7C_3 (001) and $(1\bar{1}0)$ surfaces are shown in Figure 7 and Figure 8, respectively.

As shown in Figures 5a and 6, though the CO dissociation and the adsorption site of dissociated pieces are different for the CO direct dissociation and H-assisted dissociation (to HCO or COH) pathways, the three pathways show similar reaction barriers (around 2.9 eV) on the 3F1 site of the 1Co-doped (001) surface. For the 2F3 site on the 2Co1-doped hcp-Fe_7C_3 (001) surface, the reaction barrier of CO direct dissociation is 2.39 eV, which is lower than that of HCO formation (2.79 eV) or COH formation (3.05 eV), indicating CO direct dissociation is the favorable reaction pathway. Moreover, CO hydrogenation to HCO and COH are both endothermic.

On the 2Co2-doped hcp-Fe_7C_3 (001) surface, the 3F1 site is the most stable site for CO adsorption with the binding energy of -2.61 eV, thus the CO dissociation pathway on the 3F1 site is discussed. The reaction barrier of CO direct dissociation is 2.73 eV, while it is 1.96 eV and 2.09 eV for the HCO and COH pathways, respectively. Significantly, the H-assisted dissociation to HCO on the 3F1 site of the 2Co2-doped hcp-Fe_7C_3 (001) surface shows the lowest reaction barrier among the four types of Co-doped hcp-Fe_7C_3 (001)

surfaces. As shown in Figure 6, for the H-assisted dissociation to HCO pathway, the nearby activated hydrogen atom moves to the 3F1 site, reacts with the adsorbed CO molecule, and finally generates HCO species.

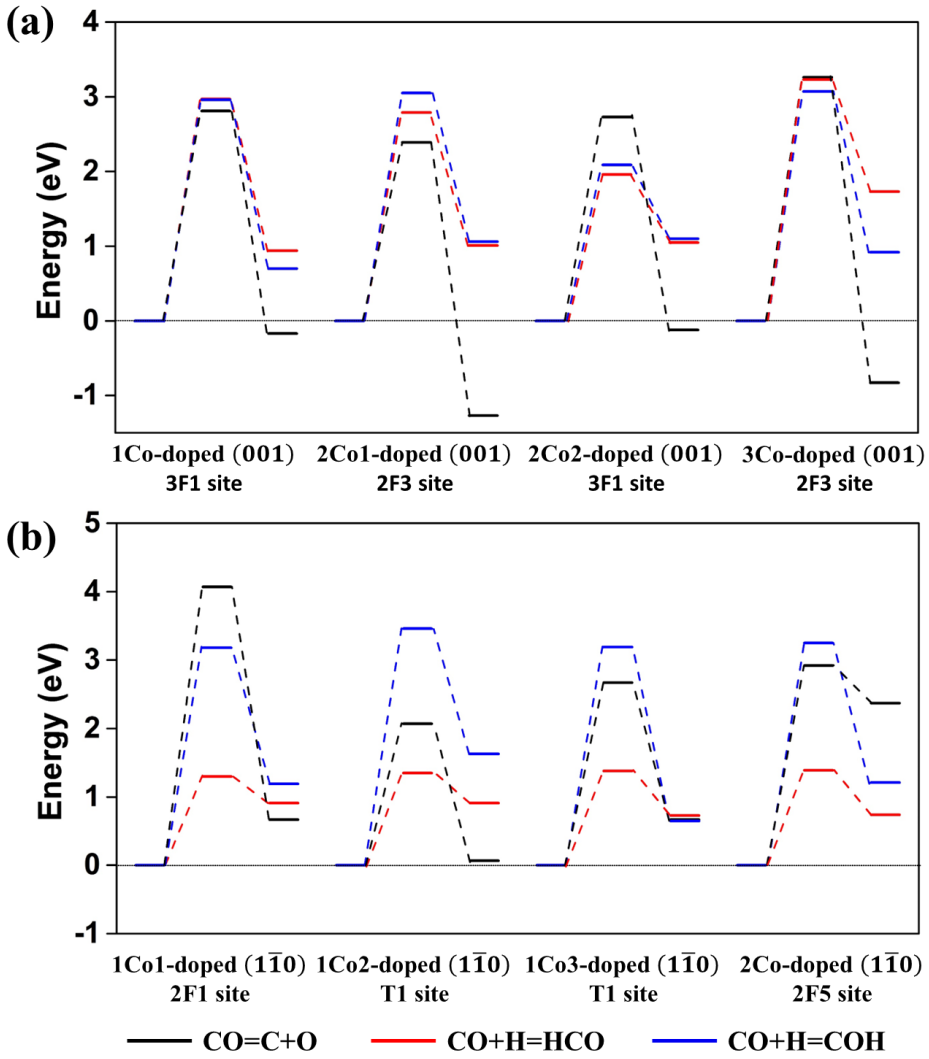

Figure 6. The potential energy diagram for the activation of CO on the Co-doped hcp-Fe_7C_3 (**a**) (001) and (**b**) (1$\bar{1}$0) surfaces.

For the 2F3 site on the 3Co-doped hcp-Fe_7C_3 (001) surface, the reaction barriers of CO direct dissociation and H-assisted dissociation to HCO and COH are 3.26 eV, 3.23 eV, and 3.07 eV, respectively. The high reaction barriers indicate both the direct dissociation and H-assisted dissociation of CO is difficult on the 2F3 site of the 3Co-doped hcp-Fe_7C_3 (001) surface. Moreover, it can be seen from Figure 5a that all the CO direct dissociation pathways on the four types of Co-doped hcp-Fe_7C_3 (001) surfaces are exothermic, while the H-assisted dissociation pathways of CO are endothermic.

On the contrary, both the CO direct dissociation and H-assisted dissociation pathways are endothermic on the four types of Co-doped hcp-Fe_7C_3 (1$\bar{1}$0) surfaces, as shown in Figure 5b. The 2F1 site is the most stable site for CO adsorption with the binding energy of −2.02 eV on the 1Co1-doped hcp-Fe_7C_3 (1$\bar{1}$0) surface, and thus the CO dissociation pathway on 2F1 site is discussed. The reaction barriers of CO direct dissociation and H-assisted dissociation to HCO and COH are 4.07 eV, 1.30 eV, and 3.18 eV, respectively. It can be seen that the direct dissociation of CO on the 2F1 site is difficult, but the H-assisted dissociation to HCO is energetically favorable. During the H-assisted dissociation of CO to the HCO pathway, as shown in Figure 7, the adsorbed activated hydrogen atom on the

2F4 site moves around the adsorbed CO molecule and finally generates HCO species on the 2F1 site. On the 1Co2-doped hcp-Fe_7C_3 $(1\bar{1}0)$ surface, the T1 site is the most stable site for CO adsorption with the binding energy of −3.26 eV, which is the lowest among the four types of Co-doped hcp-Fe_7C_3 $(1\bar{1}0)$ surfaces. For the CO dissociation on T1 site, the H-assisted dissociation to HCO is energetically favorable with the lowest reaction barrier of 1.35 eV, while the reaction barrier of H-assisted dissociation to COH is 3.46 eV. Additionally, different from the 1Co1-doped hcp-Fe_7C_3 $(1\bar{1}0)$ surface, the reaction barrier of CO direct dissociation is reduced to 2.07 eV.

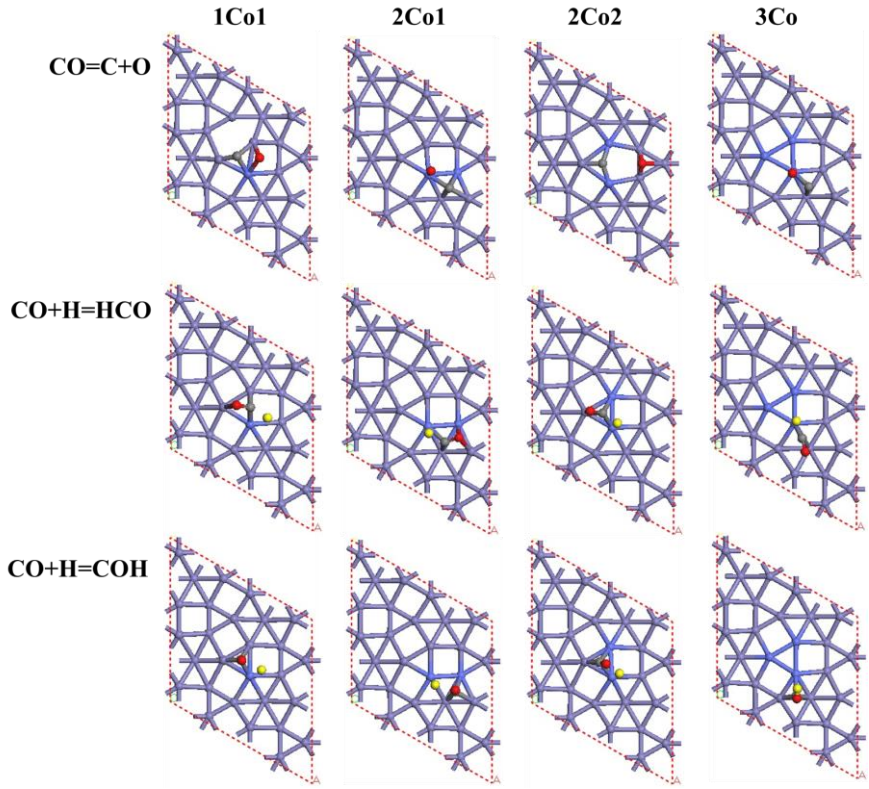

Figure 7. Structures of the transition states for CO direct dissociation and H-assisted dissociation pathways on the most stable sites of Co-doped hcp-Fe_7C_3 (001) surfaces. The Fe, Co, C, O, and H atoms are colored purple, blue, gray, red, and yellow, respectively.

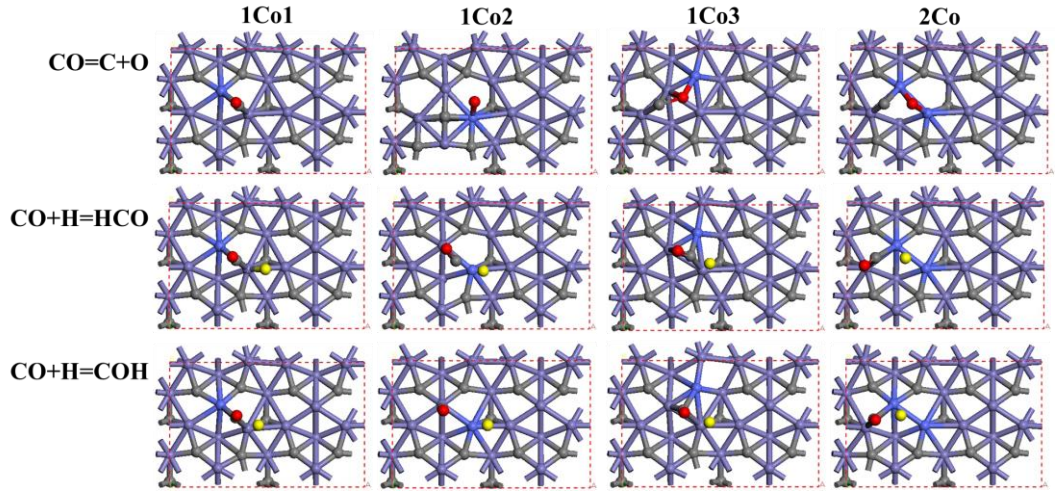

Figure 8. Structures of the transition states for CO direct dissociation and H-assisted dissociation pathways on the most stable site of Co-doped hcp-Fe_7C_3 $(1\bar{1}0)$ surfaces. The Fe, Co, C, O, and H atoms are colored purple, blue, gray, red, and yellow, respectively.

On the 1Co3-doped hcp-Fe_7C_3 $(1\bar{1}0)$ surface, the surface C atom is replaced with the Co atom, and the most stable adsorption site for CO is still the T1 site with the lowest adsorption energy of −2.33 eV. As shown in Figure 7, the reaction barrier of CO direct dissociation on this T1 site is 2.67 eV, while the H-assisted dissociation to COH has a relatively higher reaction barrier of 3.19 eV, and the H-assisted dissociation to HCO pathway just reduces to 1.38 eV. On the most stable adsorption site (2F5 site) for CO on the 2Co-doped hcp-Fe_7C_3 $(1\bar{1}0)$ surface, the reaction barriers of CO direct dissociation and H-assisted dissociation to HCO and COH are 2.92 eV, 1.39 eV, and 3.25 eV, respectively. In summary, our calculations suggest that the H-assisted dissociation to HCO is the preferred activation pathway for CO on the Co-doped hcp-Fe_7C_3 $(1\bar{1}0)$ surfaces.

3. Computational Details

All calculations in this work were conducted based on DFT and were carried out with the CASTEP package in Materials Studio of Accelrys Inc. The electron exchange and correlation energy were calculated by using the generalized gradient approximation (GGA) with the Perdew-Burke-Ernzerhof (PBE) functional [30]. The energy cutoff for the plane wave basis set was set to be 400 eV. The total energy convergence was employed as 2×10^{-5} eV/atom, while the convergence accuracy of self-consistent field was employed as 2×10^{-6} eV/atom. The k-points sampling was set as $2 \times 3 \times 1$ with the density of 0.25 $Å^{-1}$. A vacuum layer of 15 Å was set in the perpendicular direction to avoid the spurious interaction between the periodic repeating slabs for all calculations. The calculation parameters test, including supercell size, k-points, and vacuum layer, were carried out, and the calculation results indicated that the parameters employed in our work are sufficient to satisfy the computational accuracy and efficiency, as shown in Table S1.

In the present study, the crystal structure of bulk hcp-Fe_7C_3 with crystallographic parameters of a = b = 6.826 Å, c = 4.495 Å, and $\gamma = 120°$ was used as the basal structure. The Co-doped hcp-Fe_7C_3 catalysts were modeled by partial replacement of Fe or C atoms on hcp-Fe_7C_3 (001) and $(1\bar{1}0)$ surfaces with Co atoms. The adsorption behavior of CO on the Co-doped hcp-Fe_7C_3 catalysts was calculated. The adsorption energy (E_{ads}) was determined by $E_{ads} = E_{CO/slab} - E_{slab} - E_{CO}$, where $E_{CO/slab}$ is the total energy of the crystal plane absorbed with CO, E_{slab} is the energy of the crystal slab, and E_{CO} is the energy of free CO molecule.

For the dissociation of CO molecules, the transition states were located using the LST/QST method in CASTEP [31]. The reaction energy (ΔE_r) was calculated by $\Delta E_r = E(FS) - E(IS)$, while the reaction barrier (E_a) was calculated by $E_a = E(TS) - E(IS)$, where E(IS), E(TS), and E(FS) are the energies of the corresponding initial state (IS), transition state (TS), and final state (FS), respectively.

4. Conclusions

In this work, a systematically periodic DFT study was performed to understand the effect of Co doping on the adsorption and activation of CO on Co-doped hcp-Fe_7C_3 catalysts. It is found that the surface structure of the (001) surface remains basically unchanged after doping with Co atoms, while the replacements of Fe or C atoms on $(1\bar{1}0)$ surfaces with Co atoms have a significant impact on the surface structure. The top sites on the doped Co atoms of hcp-Fe_7C_3 are disadvantages for the CO adsorption, whereas the T, 2F, or 3F site around the doped Co atoms are beneficial to promote the adsorption of CO. The CO direct dissociation pathways on the four types of Co-doped hcp-Fe_7C_3 (001) surfaces are exothermic, while the H-assisted dissociation pathways of CO are endothermic. The H-assisted dissociation to HCO on the 3F1 site of 2Co2-doped hcp-Fe_7C_3 (001) surface show the lowest reaction barrier of 1.96 eV. For the Co-doped hcp-Fe_7C_3 $(1\bar{1}0)$ surfaces, the H-assisted dissociation to HCO is the preferred activation pathway for CO on the Co-doped surfaces with the reaction barrier of approximately 1.30 eV.

Supplementary Materials: The following supporting information can be downloaded at: https://www.mdpi.com/article/10.3390/catal13030564/s1, Table S1: The k-point, supercell and vacuum test for the surface calculation.

Author Contributions: Conceptualization, Y.D. and W.L.; Data curation, Y.D. and H.D.; Formal analysis, Y.D.; Methodology, Y.D.; Software, Y.D. and H.S.; Supervision, W.L.; Writing—original draft, Y.D.; Writing—review & editing, W.L. All authors have read and agreed to the published version of the manuscript.

Funding: This research was funded by the National Natural Science Foundation of China (Grant No. 21773132 and 12004210).

Data Availability Statement: The original contributions presented in the study are included in the article; further inquiries can be directed to the corresponding author.

Conflicts of Interest: The authors declare no conflict of interest.

References

1. Fischer, F.; Tropsch, H. The preparation of synthetic oil mixtures (synthol) from carbon monoxide and hydrogen. *Brennst. Chem.* **1923**, *4*, 276–285.
2. Khodakov, A.Y.; Chu, W.; Fongarland, P. Advances in the development of novel cobalt Fischer-Tropsch catalysts for synthesis of long-chain hydrocarbons and clean fuels. *Chem. Rev.* **2007**, *107*, 1692–1744. [CrossRef] [PubMed]
3. Dry, M.E. The fischer-tropsch process: 1950–2000. *Catal. Today* **2002**, *71*, 227–241. [CrossRef]
4. Dry, M.E. Present and future applications of the Fischer–Tropsch process. *Appl. Catal. A Gen.* **2004**, *276*, 1–3. [CrossRef]
5. Weststrate, C.; Van De Loosdrecht, J.; Niemantsverdriet, J. Spectroscopic insights into cobalt-catalyzed Fischer-Tropsch synthesis: A review of the carbon monoxide interaction with single crystalline surfaces of cobalt. *J. Catal.* **2016**, *342*, 1–16. [CrossRef]
6. Van Der Laan, G.P.; Beenackers, A. Kinetics and selectivity of the Fischer-Tropsch synthesis: A literature review. *Catal. Rev. Sci. Eng.* **1999**, *41*, 255–318. [CrossRef]
7. De Smit, E.; Weckhuysen, B.M. The renaissance of iron-based Fischer-Tropsch synthesis: On the multifaceted catalyst deactivation behaviour. *Chem. Soc. Rev.* **2008**, *37*, 2758–2781. [CrossRef]
8. Wang, H.; Zhou, W.; Liu, J.-X.; Si, R.; Sun, G.; Zhong, M.-Q.; Su, H.-Y.; Zhao, H.-B.; Rodriguez, J.A.; Pennycook, S.J. Platinum-modulated cobalt nanocatalysts for low-temperature aqueous-phase Fischer-Tropsch synthesis. *J. Am. Chem. Soc.* **2013**, *135*, 4149–4158. [CrossRef]
9. Zhang, Q.; Kang, J.; Wang, Y. Development of novel catalysts for Fischer-Tropsch synthesis: Tuning the product selectivity. *ChemCatChem* **2010**, *2*, 1030–1058. [CrossRef]
10. De Smit, E.; Cinquini, F.; Beale, A.M.; Safonova, O.V.; van Beek, W.; Sautet, P.; Weckhuysen, B.M. Stability and Reactivity of $\epsilon-\chi-\theta$ Iron Carbide Catalyst Phases in Fischer−Tropsch Synthesis: Controlling μ_C. *J. Am. Chem. Soc.* **2010**, *132*, 8–14941.
11. Torres Galvis, H.M.; Bitter, J.H.; Davidian, T.; Ruitenbeek, M.; Dugulan, A.I.; de Jong, K.P. Iron particle size effects for direct production of lower olefins from synthesis gas. *J. Am. Chem. Soc.* **2012**, *134*, 16207–16215. [CrossRef]
12. Schweicher, J.; Bundhoo, A.; Kruse, N. Hydrocarbon chain lengthening in catalytic CO hydrogenation: Evidence for a CO-insertion mechanism. *J. Am. Chem. Soc.* **2012**, *134*, 16135–16138. [CrossRef]
13. Borg, O.; Dietzel, P.D.; Spjelkavik, A.I.; Tveten, E.Z.; Walmsley, J.C.; Diplas, S.; Eri, S.; Holmen, A.; Rytter, E. Fischer-Tropsch synthesis: Cobalt particle size and support effects on intrinsic activity and product distribution. *J. Catal.* **2008**, *259*, 161–164. [CrossRef]
14. Xiang, Y.; Barbosa, R.; Kruse, N. Higher alcohols through CO hydrogenation over CoCu catalysts: Influence of precursor activation. *ACS Catal.* **2014**, *4*, 2792–2800. [CrossRef]
15. Liu, X.-W.; Cao, Z.; Zhao, S.; Gao, R.; Meng, Y.; Zhu, J.-X.; Rogers, C.; Huo, C.-F.; Yang, Y.; Li, Y.-W. Iron carbides in Fischer-Tropsch synthesis: Theoretical and experimental understanding in epsilon-iron carbide phase assignment. *J. Phys. Chem. C* **2017**, *121*, 21390–21396. [CrossRef]
16. Xu, K.; Sun, B.; Lin, J.; Wen, W.; Pei, Y.; Yan, S.; Qiao, M.; Zhang, X.; Zong, B. ε-Iron carbide as a low-temperature Fischer-Tropsch synthesis catalyst. *Nat. Commun.* **2014**, *5*, 5783. [CrossRef]
17. Li, Y.; Li, Z.; Ahsen, A.; Lammich, L.; Mannie, G.J.; Niemantsverdriet, J.H.; Lauritsen, J.V. Atomically Defined Iron Carbide Surface for Fischer-Tropsch Synthesis Catalysis. *ACS Catal.* **2018**, *9*, 1264–1273. [CrossRef]
18. Chen, B.; Wang, D.; Duan, X.; Liu, W.; Li, Y.; Qian, G.; Yuan, W.; Holmen, A.; Zhou, X.; Chen, D. Charge-tuned CO activation over a χ-Fe_5C_2 Fischer-Tropsch catalyst. *ACS Catal.* **2018**, *8*, 2709–2714. [CrossRef]
19. Zhao, H.; Liu, J.-X.; Yang, C.; Yao, S.; Su, H.-Y.; Gao, Z.; Dong, M.; Wang, J.; Rykov, A.I.; Wang, J. Synthesis of iron-carbide nanoparticles: Identification of the active phase and mechanism of Fe-based Fischer-Tropsch synthesis. *CCS Chem.* **2021**, *3*, 2712–2724. [CrossRef]
20. Chang, Q.; Zhang, C.; Liu, C.; Wei, Y.; Cheruvathur, A.V.; Dugulan, A.I.; Niemantsverdriet, J.; Liu, X.; He, Y.; Qing, M. Relationship between iron carbide phases (ε-Fe_2C, Fe_7C_3, and χ-Fe_5C_2) and catalytic performances of Fe/SiO_2 Fischer-Tropsch catalysts. *ACS Catal.* **2018**, *8*, 3304–3316. [CrossRef]

21. Broos, R.J.; Zijlstra, B.; Filot, I.A.; Hensen, E.J. Quantum-Chemical DFT Study of Direct and H-and C-Assisted CO Dissociation on the χ-Fe_5C_2 Hägg Carbide. *J. Phys. Chem. C* **2018**, *122*, 9929–9938. [CrossRef] [PubMed]
22. Van Santen, R.A.; Ghouri, M.M.; Shetty, S.; Hensen, E.M. Structure sensitivity of the Fischer-Tropsch reaction; molecular kinetics simulations. *Catal. Sci. Technol.* **2011**, *1*, 891–911. [CrossRef]
23. Cheng, J.; Hu, P.; Ellis, P.; French, S.; Kelly, G.; Lok, C.M. Density functional theory study of iron and cobalt carbides for Fischer-Tropsch synthesis. *J. Phys. Chem. C* **2010**, *114*, 1085–1093. [CrossRef]
24. Yang, C.; Zhao, B.; Gao, R.; Yao, S.; Zhai, P.; Li, S.; Yu, J.; Hou, Y.; Ma, D. Construction of synergistic Fe_5C_2/Co heterostructured nanoparticles as an enhanced low temperature Fischer-Tropsch synthesis catalyst. *ACS Catal.* **2017**, *7*, 5661–5667. [CrossRef]
25. Pham, T.H.; Duan, X.; Qian, G.; Zhou, X.; Chen, D. CO activation pathways of Fischer–Tropsch synthesis on χ-Fe_5C_2 (510): Direct versus hydrogen-assisted CO dissociation. *J. Phys. Chem. C* **2014**, *118*, 10170–10176. [CrossRef]
26. Pham, T.H.; Qi, Y.; Yang, J.; Duan, X.; Qian, G.; Zhou, X.; Chen, D.; Yuan, W. Insights into Hägg Iron-Carbide-Catalyzed Fischer-Tropsch Synthesis: Suppression of CH4 Formation and Enhancement of C–C Coupling on χ-Fe_5C_2 (510). *ACS Catal.* **2015**, *5*, 2203–2208. [CrossRef]
27. Broos, R.J.; Klumpers, B.; Zijlstra, B.; Filot, I.A.; Hensen, E.J. A quantum-chemical study of the CO dissociation mechanism on low-index Miller planes of θ-Fe_3C. *Catal. Today* **2020**, *342*, 152–160. [CrossRef]
28. Zhang, M.; Ren, J.; Yu, Y. Investigating the CO activation mechanism on hcp-Fe_7C_3 (211) via density functional theory. *Mol. Catal.* **2021**, *505*, 111506. [CrossRef]
29. Fu, J.; Sun, D.; Chen, Z.; Zhang, J.; Du, H. First-Principles Investigation of CO Adsorption on h-Fe_7C_3 Catalyst. *Crystals* **2020**, *10*, 635. [CrossRef]
30. Perdew, J.P.; Chevary, J.A.; Vosko, S.H.; Jackson, K.A.; Pederson, M.R.; Singh, D.J.; Fiolhais, C. Atoms, molecules, solids, and surfaces: Applications of the generalized gradient approximation for exchange and correlation. *Phys. Rev. B* **1992**, *46*, 6671. [CrossRef]
31. Cao, D.-B.; Li, Y.-W.; Wang, J.; Jiao, H. Chain growth mechanism of Fischer-Tropsch synthesis on Fe_5C_2 (0 0 1). *J. Mol. Catal. A Chem.* **2011**, *346*, 55–69. [CrossRef]